Kinetics analysis of the electro-catalyzed degradation of high potential LiNi0,5Mn1,5O4 active materials

P. Dumaz, C. Rossignol, A. Mantoux, Nicolas Sergent, R. Bouchet

Kinetics analysis of the electro-catalyzed degradation of high potential $LiNi_{0,5}Mn_{1,5}O_4$ active materials

P. Dumaz[a], C. Rossignol[a], A. Mantoux[b], N. Sergent[a] and R. Bouchet[a*]

[a] Univ. Grenoble Alpes, Univ. Savoie Mont Blanc, CNRS, Grenoble INP, LEPMI, 38000 Grenoble, France

[b] Univ. Grenoble Alpes, CNRS, Grenoble INP, SIMaP, 38000 Grenoble, France

renaud.bouchet@lepmi.grenoble-inp.fr

Abstract

One approach to increase the energy density of Li-ion batteries is to use high potential cathode material like $LiNi_{0.5}Mn_{1.5}O_4$ (LNMO). However, it suffers from low coulombic efficiency, self-discharge and poor cyclability in carbonates-based electrolytes. Many mechanisms to explain degradation such as HF generation, surface catalytic activity and transition metals dissolution have been suggested to explain these behaviors. By comparison with a non-fluorinated environment, we demonstrated that hydrofluoric acid is not the main reason of capacity loss. A comparison of electrolyte degradation on model thin-film and composite electrodes proved that electrolyte oxidation is catalyzed on the active material surface of LNMO and not on the carbon. A Tafel like behavior of the electrolyte oxidation was obtained thanks to the measure of the steady state current at different potentials. The low coulombic efficiency is essentially related to the self-discharge mechanism. Finally, the capacity fading has been quantitatively correlated to the electrolyte oxidation: at 25°C, about 4% of oxidized electrolyte molecules leads to the degradation of the material, probably due to the dissolution of surface transition metal. By lowering the operating

temperature, the electrolyte degradation kinetics decreased, leading proportionally to better cycling stability. Perspectives of this work are also drawn.

Keywords

Catalyze, spinel LNMO, capacity fading, faradic efficiency, Tafel kinetics, self-discharge

I. Introduction

The revolution of nomad electronic, all interconnected, has been made possible thanks to the improvement of electrochemical storage and especially, the invention of Li-ion technology in the nineties [1]. However, current Li-ion systems are reaching their theoretical chemical limits in term of energy density. The two mean levers to increase the energy density are 1/the increase of the capacity density, and 2/ the increase of the battery voltage. One of the main short-term solution is to develop cathode material with higher potentials than conventional cathode based on lamellar $LiMO_2$ (with M=Co, Ni, Mn, Al). Among these new materials, we can cite the Li-rich family $Li_{(1+x)}MO_2$, the high potential $LiMPO_4$ olivine, with M = Mn, Co, Ni...or the LiM_2O_4 spinel with M = Mn, Ni, Cr... [2], [3].

The spinel $LiNi_{1/2}Mn_{3/2}O_4$ (LNMO) presents a particular interest because of its high operating voltage (> 4.7 V vs Li^+/ Li) [4], resulting from successive oxidation of Ni^{II} to Ni^{III}, then to Ni^{IV} [5], associated with a theoretical specific capacity of 147 $mAh.g^{-1}$, which offers a theoretical specific energy of approximately 650 $Wh.kg^{-1}$ of active material (AM), when faced to lithium metal negative electrode [6]. Moreover, considering other aspects such as cost, sourcing and eco-development, the LNMO is a very interesting material [7]. Indeed, the synthesis of LNMO is easy and cost effective [8]. Nowadays, a strong effort is made to reduce the cobalt

content in the standard lamellar compound $LiCoO_2$ based on Co substitution (Ni, Mn, Al) with the famous NMC or NCA. Mn is abundant and presents low toxicity, and LNMO offers us a Co-free active material, which makes it eco-friendlier. According to the synthesis method, LNMO presents two different crystal structures [9]; one called disordered because the transition metals are distributed randomly in the structure, while the ordered structure presents a periodic arrangement (super-structure) [10]. The nickel is at the +II oxidation state whereas the Mn is generally +IV [5]. Depending on the oxygen vacancies content, the oxidation degree of Mn can be slightly lower than +IV [11], which leads to slight variations in the electrochemical properties of the material, especially with a small plateau around 4,1 V vs Li+/Li [5].

However, crucial challenges must be solved to enable its commercial use in Li-ion battery: when cycled, LNMO suffers from a low coulombic efficiency (usually in-between 90 to 99% [12], [13]) and a continuous capacity fading [14]. When stored in a full-charged state in calendar conditions, a pronounced self-discharge is observed [15]. In addition, the post-mortem chemical analysis (ICP, XPS) of the electrolyte and the Solid Electrolyte Interphase (SEI) of the negative electrode reveals the dissolution of Ni and Mn transition metals from the structure [16], and demonstrates the slow degradation of the LNMO. These phenomena are aggravated when the temperature increases [17]. The scientific community tried to solve these problems using different approaches. Among them, the addition in the electrolyte of additives (LiBOB, FEC, succinic anhydride, lithium malonatoborate to cite a few [15], [18], [19]) is a common approach. The idea is to form a protective film onto the electrode surface (Cathode Electrolyte Interphase, CEI) allowing to limit the parasitic reactions, *i.e.* the electrolyte oxidation and the AM dissolution. The CEI can also be realized *ex situ* by adequate coating methods (ALD, evaporation, electroless plating, sol-gel…) of the AM surface with a

more stable compounds, e.g. Al_2O_3, $LiNbO_3$ [20], [21]. At last, the substitution of the Ni/Mn by other transition metals (Al, Mg, Fe) has been also used to stabilize the AM surface [6], [22], [23]. Most of these complex material engineering processes have generally brought limited improvement [21], in particular the cyclability remains quite poor and the material dissolution has not been tackle until now. This can be partly explained by the fact that the complex entanglement between the electrolyte decomposition and the LNMO degradation is still not yet fully understood.

Obviously, the high operating voltage of LNMO is well above the electrochemical stability of standard electrolytes based on a mixture of carbonates laden with 1M $LiPF_6$ (lithium salt) [24], resulting in electrolyte oxidation that may produce various molecules such as aldehydes, alcohols, hydrogen fluoride, oxygen, carbon dioxide and monoxide, etc. [25], [26], [27]. This electrolyte instability and parasitic oxidations leads to the electrode deterioration [28]. Many mechanisms have been proposed in literature to explain the capacity fading. Among them, research teams suggested an intrinsic instability of the structure that suffers from fatigue after repetitive lithiation/delithiation [29], [30], or also due to the Jahn-Teller distortion, and/or disproportionation reaction that can destabilize the structure and promote Ni/Mn dissolution [11], [31]. The formation of isolating surface film due to the accumulation of degradation by-products at the CEI, formed by repetitive oxidation of electrolyte may reduce the cyclability of LNMO [16]. There is also a fairly recurrent mechanism involving *in situ* generated fluorhydric acid (HF) which attacks the active material [21], [32]. More recently, Kostecky *et al.*, based on previous work by Kumar *et al.* on $LiMn_2O_4$, demonstrated the catalytic activity of the LNMO surface against a carbonate based electrolyte. Indeed, the presence of oxygen deficiencies and Mn^{III} modifies the local surface charge density distribution. This particular arrangement of the surface exhibits a catalytic oxidation of carbonate solvents

which is usually accompanied by reduction/dissolution of the transition metals. This dissolution is carried out thanks to β-diketonate ligands, generated by oxidation of electrolyte solvents, which complex and solubilize the Mn(II/III) and Ni(II) surface TM cations [26], [25].

The relative impact of each mechanism is always under debate and their kinetics are unknown. Herein, we compare the electrochemical behaviour of two configurations: an LNMO model thin layer without binder nor carbon additives, and a standard composite electrode. With the thin film electrode, the comparison of fluorine-free electrolyte (EC/DMC 50:50 vol. laden with 1M $LiClO_4$) versus standard LP30 electrolyte with $LiPF_6$ in place of $LiCLO_4$, permits to evaluate the influence of the HF formation on the degradation kinetics. The comparison of carbon-free electrodes based on the thin film electrode and composite electrodes proves the catalytic effect of LNMO surface on the electrolyte degradation. The kinetics of this oxidation mechanism is measured and a corrosion process following a Tafel law is obtained. Varying the temperature, we demonstrate a strong correlation between the carbonate oxidation kinetics and the LNMO capacity fading, which confirms that the mean mechanism for the LNMO performance fading is due to carbonate oxidation by-products as chelating agents of the transition metal Mn/Ni as proposed by of Kumar *et al.* and Jarry *et al.* [26], [25]. The comparison of the two kinetics gives a tool that allows the quantitative estimation of the LNMO material fading only knowing the faradic efficiency of the charge/discharge. Finally, simple rules are deduced from our findings to design LNMO materials with improved cyclability.

II. Materials and Methods

II.1. LNMO thin film

Thin films were prepared by electrostatic spray deposition [33]. $LiNO_3$ (purity = 99%, Strem Chemical), $Mn(NO_3)_2 \cdot 4H_2O$ (purity = 98.5%, Merck) and $Ni(NO_3)_2 \cdot 6H_2O$ (Purity = 99%, Aldrich) precursors were dissolved in a 50:50 H_20/Buthylcarbitol (Alfa Aesar) ratio, in stoichiometric proportions to target the composition $LiNi_{0.5}Mn_{1.5}O_4$.

A 10 ml syringe associated with a syringe-pump allowed a flow of the solution of 1 $mL.h^{-1}$. High DC voltage of 10 kV was applied between the needle and the stainless steel (SS) substrate holder, leading to the generation of a spray. The substrate (0,5 mm thick, 16 mm diameter 316L stainless steel disk) placed at a distance of 30mm from the needle, was heated at 200°C. Finally, 80 min of deposition in these conditions were used. After deposition, a calcination in air at 600°C for 1h lead to the formation of the LNMO thin film (14mm of diameter). The AM mass was determined by weighting the substrate before and after deposition. A weight of 0.95 ± 0.05 mg was reproducibly obtained. The thickness of the layer was 2 µm, as shown by cross section imaging using SEM (see fig. S1 in SI). The layer was not perfectly compact and some residual porosity existed. Furthermore, the presence of an interlayer (<200nm) between LNMO and SS substrate, due to the diffusion of stainless steel components (Cr, Ni, Fe) in the layer during the calcination, was observed [34] and characterized by TEM-EDX (see fig. S1 in SI). This interlayer, made of Ni/Fe/Cr oxides, corresponded to approximately 20% of the mass of the thin film, and thus the active LNMO mass of the thin film was closer to 0.75 mg.

II.2. LNMO powders

$LiNO_3$ (purity = 99%, Strem Chemical), $Mn(NO_3)_2 \cdot 4H_2O$ (purity = 98.5%, Merck) and $Ni(NO_3)_2 \cdot 6H_2O$ (Purity = 99%, Aldrich) precursors were dissolved in stoichiometric proportion in 5 mL of distilled water. The pH was adjusted to 7.5 by adding ammonia, then the solution was placed in an ultrasonic bath (Crest Tru-sweep 275HT, 80W) for 5 hours at 80°C. After partial evaporation of the water, the slurry was placed into an alumina crucible in a furnace and heated at 800°C for 24h. Finally, the obtained powder was ground to reduce the size of agglomerates.

II.3. Material Characterizations

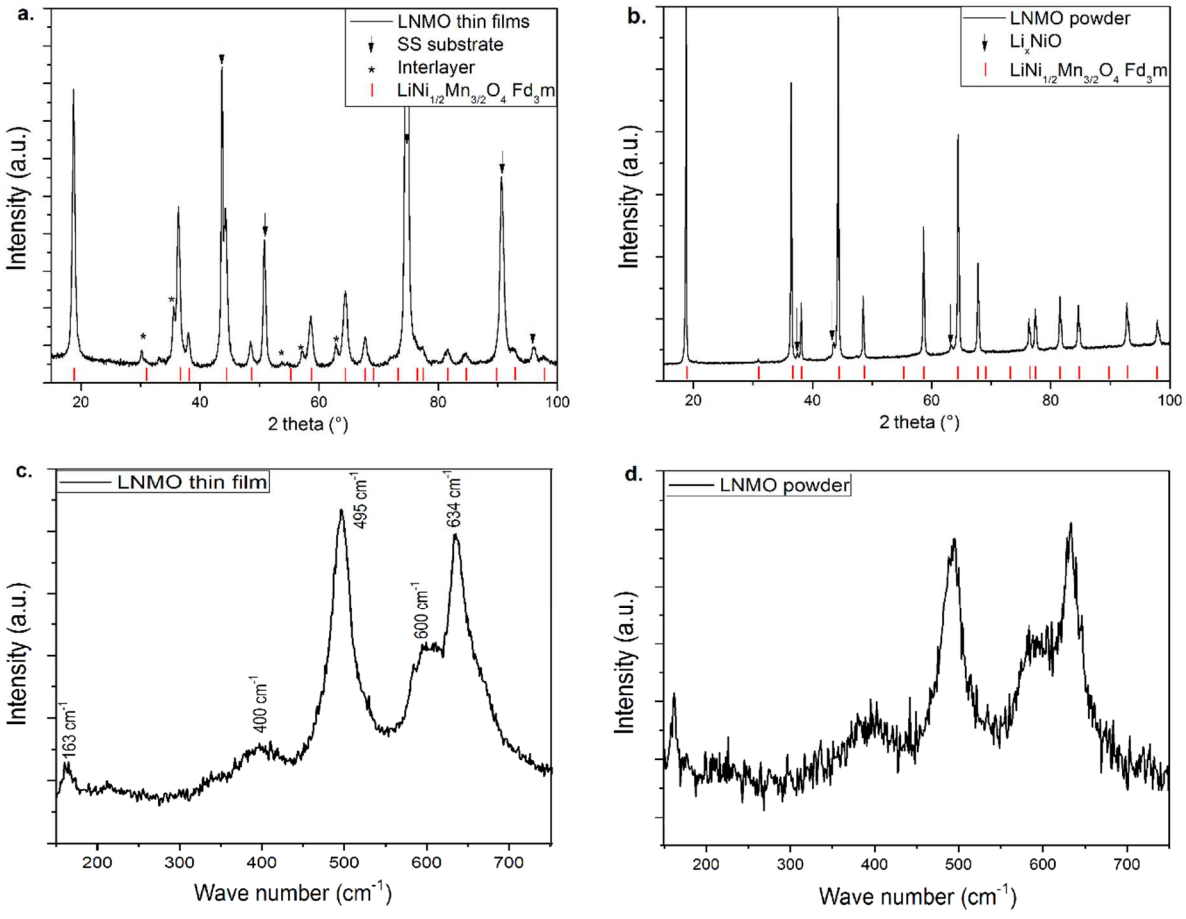

Figure 1 : XRD diffractograms and Raman spectra of the LNMO thin film on SS substrate after calcination at 600°C / 1h (a, c), and of the LNMO powder after calcination at 800°C / 24h (b, d).

XRD diffractograms were obtained on a X'Pert Pro MPD (PANalytical) in reflexion mode. For thin films, acquisition was performed in grazing mode, while on powder, acquisition was in Bragg-Brentano configuration (λ=1.54 Å). Raman spectra have been obtained with a Renishaw InVia spectrometer in micro-Raman configuration (objective x50) equipped with a Peltier cooled CCD detector. A 514 nm excitation have been used at a power less than 3 mW onto the sample in order to minimize local heating. Figure 1 presents the structural characterization by XRD and Raman spectroscopy of the synthesized LNMO as thin film (a, c) or powder (b, d). XRD on thin film reveals the majority presence of LNMO phase with Fd3m structure. Fairly large peaks are obtained compared to the LNMO powder, which reflects a smaller crystallite size in the thin film than in the powder. This result is not surprising considering the deposition process and the low temperature and duration of the calcination. An interlayer phase consisting of mixed transition metal oxides, due to the diffusion of this elements from the SS substrate to the film during calcination, is also observed. The XRD on LNMO powder shows that the major phase is LNMO in Fd3m structure, with the presence of lithiated nickel oxide impurities.

LNMO spinels can crystallize in two types of structure, an ordered $P4_332$ phase and a disordered Fd3m phase, depending on the ordering of the transition metals Ni/Mn in the octahedral sites **[35]**. The transition between ordered and disordered phases is correlated with both calcination atmosphere and temperature. According to Amatucci *et al*. **[9]**, under air, a temperature between 600 and 700°C should lead to the ordered phase, while at more elevated temperatures, to the disordered structure. Raman spectroscopy is sensitive through phonon modes to the long-range ordering of the structure. The bands at 630 and 600 cm^{-1}

are mainly due to Mn-O vibrations in a cubic structure, while those at 495, 400 and 163 cm^{-1} are mainly attributed to Ni-O vibrations **[36]**, **[37]**. According to Amatucci *et al*. **[9]**, it is possible to differentiate disordered (Ni/Mn) and ordered structure from the Ni-O bands, namely 166 and 410 cm^{-1}, that become more intense, sharper and better resolved in the ordered structure. The Raman spectra indicate that on both powder and thin film, the major phase is a disordered Fd3m structure in good agreement with XRD results. For the powder, this result is coherent with the applied calcination temperature (800°C). For thin film, one could expect an ordered structure due to the 600°C calcination temperature, but the sintering time was really short (1h), which probably did not left enough time for Ni and Mn to order over a sufficiently long range.

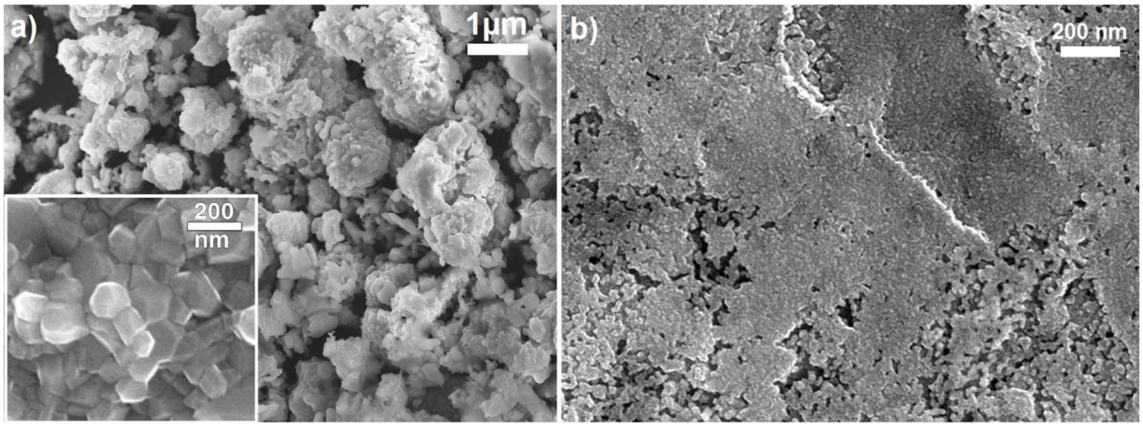

Figure 2 : SEM pictures of LNMO powder (a) and surface of thin film (b).

SEM pictures of LNMO powder and thin film, conducted on a MEB-FEG Zeiss ultra 55, are shown in figure 2. For the powder, quite dense micrometric particles consisting of sintered smaller grains around 200 nm are observed. The BET [38] specific surface of the powder has been measured by N_2 adsorption. A value of 0.8 $m^2.g^{-1}$ were obtained, which corresponds to the specific surface of 1µm cubic grain (S_{spe}= 6/ρr, with ρ the LNMO density, 4,4 $g.cm^{-3}$) in good agreement with the SEM analysis. The thin film surface (fig. 2b) has a quite dense

microstructure composed of very small grains of about 15 nm, however, locally it can be found some micrometric porosity, as revealed by the cross section picture of the film (see fig. S1 in SI).

II.4. Electrodes and electrochemical tests

LNMO composite electrodes formulation were 80:10:10 wt. % of LNMO, C65 carbon, and polyvinylidenefluoride (PVDF), respectively. They were mixed using ultra-turrax (IKA T25) with N-methylpyrrolidone (NMP) till the slurry became homogenous, and finally, coated onto an Al foil with a Dr. Blade. The electrode was dried at 80 °C for 12h, and another 12h under argon atmosphere to fully remove the NMP solvent. Then, composite electrodes were cut into 12mm disks and stored in a glove box (Jacomex, O_2, H_2O<1ppm) before battery assembly. Four different loadings were prepared: 1.75, 1.9, 2.45, and 2.8 mg.cm^{-2}. For coin cell assembly, thin films deposited on SS substrates were directly used as cathode (14mm diameter of AM) and current collector, respectively. For both composite and thin film batteries, two layers of separator (Celgard, Viledon) and a 1 M $LiPF_6$ in ethylene carbonate (EC)/dimethyl carbonate (DMC) (1:1vol. ratio) electrolyte (commercial LP30, Solvionic) were used. For the preparation of non-fluorinated electrolyte (1M $LiClO_4$ EC/DMC), $LiClO_4$ salt, dried 72h at 80°C under vacuum, was dissolved in ethylene carbonate (EC)/dimethyl carbonate (DMC, both battery grade) at a 1:1vol. ratio. Water content measured by Karl Fisher (Titroline 7500 KF) was < 20 ppm H_2O. Finally, a lithium foil acted as the counter and reference electrode.

Electrochemical tests were performed using a VMP300 (BioLogic) multichannel potentiostat. Composite electrodes were cycled between 3 and 5 V vs Li^+/Li at a C/3, D/2 rate, while thin films were cycled between 3.5 and 5 V vs Li^+/Li at a C/5 D/5 rate. Before these cycling tests, five formation cycles were usually realized at C/5, D/5 to obtain the practical capacity of the

electrodes and a stable SEI on lithium. The non-faradic currents (due to parasitic reactions) as function of the potential were measured by chonopotentiometric experiments. After the 5 formation cycles, cathodes were charged at C/5 until the desired potential, where they were held for 5 hours. The current decreased until it reached a residual steady-state value due to the non-faradic processes. Finally, for self-discharge experiments, the cathodes were fully charged at C/5 until 5V vs Li^+/Li, then leaved in open-circuit condition and the time-evolution of the voltage was recorded. All the experiments were realized at controlled temperatures (5, 10 or 25°C) thanks to an IPP30 chamber (Memmert) or a climatic chamber (CTS).

III. Results and discussion

III.1. Is the Fluor the real tread?

In order to check the impact of the Fluor, Fluor-free batteries were assembled using thin LNMO films and a Fluor-free electrolyte made of EC/DMC 1:1 laden with 1M $LiCLO_4$ (H_2O < 20 ppm). Their cycling characteristics were compared to reference cells made using LNMO thin film with a standard fluorinated LP30 electrolyte (in SI figure S2). Above 4.9 V vs Li^+/Li, a plateau is observed with the batteries made with the $LiClO_4$ based electrolyte due to the continuous oxidation of the solvent on aluminum current collector [27]. This observation confirmed that PF_6^- leads to a better passive layer on the aluminum collector, enabling the positive electrode to reach a potential as high as 5V vs Li^+/Li (see fig. S2 in SI). To compare the cycle-life, the cut-off potential for the charge was fixed at 4.85 V vs Li^+/Li for both $LiPF_6$- and $LiClO_4$-based batteries.

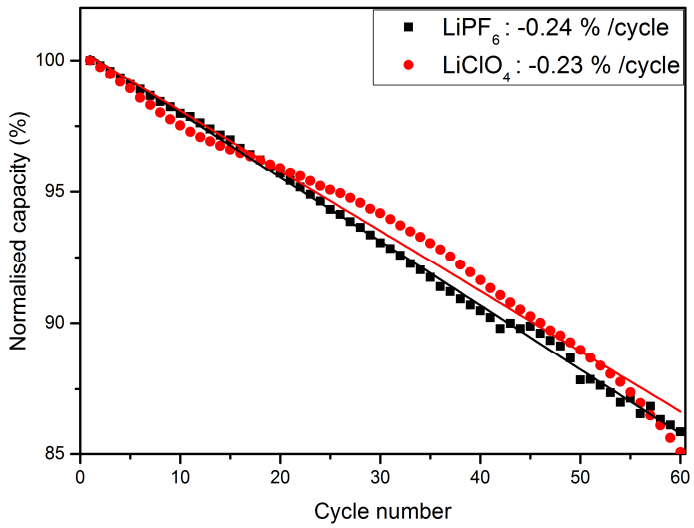

Figure 1: Normalized discharge capacity of LNMO thin film with $LiPF_6$ (black) or $LiClO_4$ (red) based electrolytes (1M in EC/DMC 1:1).

The results are shown in figure 3. A very similar capacity fading is obtained for both systems, proving that a fluorinated environment is not the main reason for the LNMO capacity fading. In addition, this result was also confirmed using composite electrodes (see fig. S3 in SI) with $LiCLO_4$ or $LiPF_6$ based electrolytes. This finding challenges the common misconception that the HF generated *in situ* is the main driving force for the degradation of the LNMO performance.

III.2. Catalytic factor

Electrolyte oxidation happens when the positive electrode reaches a potential of 4,6 V vs Li+/Li [14]. The mechanism can simply be written as [27], [15], [16]:

$$Electrolyte \rightarrow Electrolyte^{+} + e^{-} \qquad \text{eq. 1}$$

where Electrolyte and Electrolyte^{+} stand for EC, DMC and/or $LiPF_6$ in normal and oxidized forms, respectively. The positive composite electrode is mainly composed by the active material, PVdF binder, and C65 conductive carbon. Nano-sized carbon additives are added in

composite electrodes to correctly “wire” electrically the grains of AM to the current collector. Due to their nanoscale, they greatly contribute to the total electrical surface of the electrode. For example, the specific surface of the C65, use herein to formulate the composite electrodes, is 65 $m^2.g^{-1}$. Therefore, according to the electrode formulation and specific surface of the LNMO and C65, almost 90% of the electrode surface is made of carbon.

In order to check if these carbon additives are involved into the electrolyte oxidation, we compared the non-faradic current, I_{cor}, obtained on thin films (without carbon) and on composite electrodes (with 10% carbon). I_{cor} expresses the amount of current dedicated to a parasitic reaction such as electrolyte oxidation, and can be estimated thanks to the faradic efficiency using the following model. When the battery is charged at constant current (I_c), most part, $I_{f,c}$, is due to the faradic reaction of active material (LNMO) de-intercalation, while the residual part, $I_{cor,c}$, is due to the parasitic reactions (*e. g.* electrolyte degradation, aluminum current collector corrosion) such as:

$$I_c = \mathrm{I_{f,c}} + \mathrm{I_{cor,c}} \qquad \text{eq. 2}$$

We can express the discharge current following the same structure with I_d the discharge current:

$$I_d = I_{f,d} + I_{cor,d} \qquad \text{eq. 3}$$

Assuming reasonably that the intercalation/deintercalation processes are reversible, we can express the faradic capacity (C_F):

$$C_F = I_{f,c} \cdot tc = I_{f,d} \cdot td \qquad \text{eq. 4}$$

With t_c and t_d the charge and discharge time, respectively. Combing eq.2, 3 and 4 we obtain:

$$I_c \times t_c - I_d \times t_d = I_{cor,c} \times t_c - I_{cor,d} \times t_d \qquad \text{eq. 5}$$

The faradic efficiency η_{far} is expressed as the ratio of the discharged capacity (C_D) on the charged capacity (C_c):

$$\eta_{far} = C_D/C_c = I_d \times t_d/I_c \times t_c \quad \text{eq. 6}$$

If we combine eq. 5 and 6, we obtain the following expression for the corrosion current:

$$I_{cor,c} = I_c \times (1-\eta) + I_{cor,d} \times t_d/t_c \approx \mathrm{I_c} \times (1-\eta) \quad \text{eq. 7}$$

Knowing that the discharge happens at a lower potential than the charge, and considering that the parasitic oxidation current density follows a Tafel dependence with an exponential activation with the potential [24], [39], [40], the corrosion current during discharge ($I_{cor,d}$) will be small compared to the one in charge. Moreover, in our set of experiments the discharge is always made at higher rate than the charge so the term t_d/t_c will always be inferior to 1.

Therefore, the term with $I_{cor,d}$ can be, in a first approximation, neglected leading to a very simple estimation of $I_{cor} \approx I_{cor,c}$. This assumption leads to a constant underestimation of the corrosion current, but the relative evolution of the latter, depending on the different parameters like temperature or rate for example, remains valid.

Taking into account eq. 7, the table 1 summarizes the values of the faradic efficiencies and the calculated average corrosion current densities, i_{cor}, as function of the charge rate. $i_{cor} = I_{cor} / S$ has been calculated using either the total electroactive surface of electrode (S_{EA} = carbon + AM for composite electrodes) or by the AM surface only (S_{AM}). For composite electrodes, the electroactive surface is estimated as the sum of the AM and carbon surfaces estimated by BET (0,8 and 65$m^2.g^{-1}$, respectively). Very interestingly, from table 1, it appears that the values of the average corrosion current densities normalized by the AM surface are globally independent of the rate till C/3, and especially are quite close for thin films and composite electrodes. For composite electrodes, If the kinetics of oxidation of the electrolyte have been similar on carbon or LNMO surface, a roughly 10-time higher corrosion current densities

would have been expected for composite electrodes, compared to the thin films, which is far from being the case. This result demonstrates that the kinetics of oxidation of electrolyte on the carbon surface is almost negligible compared to the ones on LNMO surface: most part of the corrosion current density, i_{cor}, comes from the AM/electrolyte interfaces.

Current density ($\mu A.cm^{-2}$)	Rate	Coulombic efficiency (%)	i_{cor} ($\mu A.cm^{-2}$ of electroactive surface, S_{ea})	i_{cor} ($\mu A.cm^{-2}$ of AM, S_{AM})
Composite electrodes (variable loading)				
14.7	C/20	86.8	$1.24x10^{-2}$	0.14
17.7	C/15	87.8	$1.38x10^{-2}$	0.15
29.5	C/10	89.2	$2.04x10^{-2}$	0.23
44.2	C/6	95.3	$1.13x10^{-2}$	0.15
86.5	C/3	96.6	$1.73x10^{-2}$	0.19
Thin films				
4.5	C/20	79.8	0.23	0.23
9.1	C/10	88.1	0.27	0.27
23.8	C/4	94.2	0.22	0.22
91.9	C	97	0.45	0.45

Table 1 : Coulombic efficiencies and calculated corrosion current densities normalized either by the total electroactive surface or by the active material surface, for composite electrodes and thin films at different rates.

This results confirms that the electrolyte oxidation is catalyzed by the LNMO surface as proposed by Kostecky *et al.* and Kumar *et al.* [25], [26]. Therefore, a common approach to tackle this interfacial issue, is the surface coating by an ultra-thin dense buffer layer composed of Al_2O_3, AlF_3, etc. [41], [42], [43], [44]. Among all the parameters for the choice of the coating chemistry like chemical and electrochemical stability, ionic and electronic conductivity, we suggest to add the catalytic factor for the oxidation of the electrolyte.

III.3. Kinetics analysis of the electrolyte degradation

During the cycling tests, the efficiency decreases strongly when the rate is lowered (see table1), which supports the fact that the competition between faradic and non-faradic processes is more important when the applied current is small. To quantify i_{cor} as function of the positive electrode potential, we measured at 25°C the residual steady-state current densities (i. e. normalized by the AM surface only) after 5h of holding at different potentials, for both composite and thin film LNMO electrodes. All the results are plotted in Tafel coordinates in figure 4.

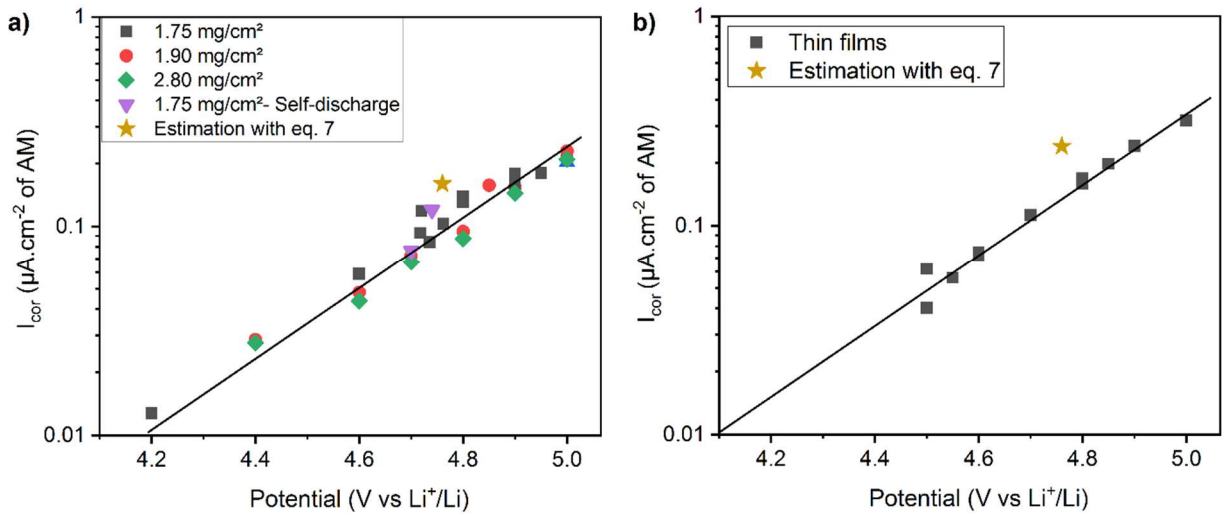

Figure 4: Steady-state current densities, namely i_{cor}, obtained at different potentials after 5h of floating at 25°C for different loadings of composite electrodes of LNMO (a), and for thin films of LNMO (b). Each point is normalized by the surface of active materials only.

Interestingly, whatever the AM loading (fig. 4a) in the composite electrodes, all the data follow the same mother curve, and i_{cor} values are on the same range for thin films and composite electrodes, which further confirms that i_{cor} depends only on the LNMO exposed surface. In addition, the corrosion current density obtained above 4.7V vs Li^+/Li are rather in good agreement with the estimated average values using our simple model (eq. 7) with the faradic efficiency (stars in fig. 4). In this representation, the corrosion current density values follow a linear behavior for both electrode microstructures, which corresponds to a Tafel law:

$$i_{cor} = i_{0,cor} exp^{(\alpha nFE/RT)} \qquad \text{eq. 8}$$

Straight lines stand for the best fits of datasets using eq. 8. If we admit a single electron mechanism for the EC oxidation [45], so n=1, we find the same coefficient of symmetry, α = 0.1, for both thin films and composites.

However, the exchange current density, $i_{0,cor}$, obtained on thin films is slightly higher ($1.2x10^{-9}$ $\mu A.cm^{-2}$) than the one obtained on composites ($8.5x10^{-10}$ $\mu A.cm^{-2}$), similarly to the estimated values from the model (eq.7, see Fig. 4). This can be explained 1/ by an underestimation of the AM surface in the composite electrode due to the partial coating of the LNMO particles by the PVdF binder, and 2/ by the different microstructures of LNMO material in the two types of electrodes, such as exposed facets, sizes of the crystallites, surface defects, which are known factors that impact the LNMO's surface activity.

III.4. Correlation with Self-discharge

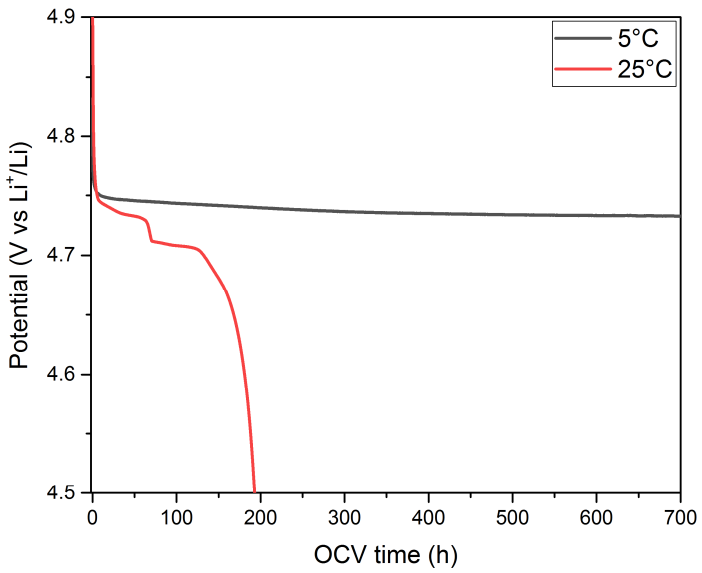

Figure 5: Characteristic self-discharge curves obtained on fully charged LNMO (NMO) composite electrodes at two temperatures : 5° and 25°C.

Figure 5 represents the evolution of the voltage of batteries left in open circuit condition after a full recharge either at 25 or at 5°C. In these conditions, the open circuit voltage (OCV) continuously drops, testifying of self-discharge mechanisms. The self-discharge mechanism can be simply expressed as the coupling between the electrolyte oxidation (eq. 1) and the NMO reduction [27], [15], [16] (Eq. 9):

$$Electrolyte \longrightarrow Electrolyte^{+} + e^{-} \quad \text{eq. 1}$$

$$Ni_{0.5}Mn_{1.5}O_4 + Li^{+} + e^{-} \longrightarrow LiNi_{0.5}Mn_{1.5}O_4 \quad \text{eq. 9}$$

where $Ni_{0.5}Mn_{1.5}O_4$ stands for the delithiated spinel, Electrolyte and Electrolyte$^+$ stand for EC, DMC and/or $LiPF_6$ in normal and oxidized forms, respectively. Knowing the capacity of the electrode, C_F, we deduced from these self-discharge curves an associated self-discharge current, calculated by dividing the capacity by the time taken for the material to be fully discharged. This can be done for each potential plateau. The obtained values are 0.12 µA.cm^{-2} for the first plateau at a mean potential of 4.74 V vs Li^+/Li, and 0.077 µA.cm^{-2} for the one below located of 4.7 V vs Li^+/Li. These values have been added in Fig. 4 and they fit really well with the mother curve of i_{cor} measured at imposed potentials. This is very satisfactory that the three different methods, i. e. the faradic efficiencies (eq. 7), the steady state currents measured in potentiostatic mode or the self-discharge experiments give the same results: the main parasitic reaction is the oxidation of the electrolyte on the surface of the active material. On figure 5 is also plotted the evolution at 5°C of the self-discharge potential for the same composite electrode. The potential quickly drops to 4.75 V vs Li^+/Li then reach a very stable plateau, taking 700h to lose 0.1 V. This shows that the self-discharge reaction, i. e. the electrolyte oxidation is thermally activated, as expected through the term $i_{0,cor}$ in Tafel law (eq. 8). Thus, the electrochemical stability of commercial LP30 on LNMO surface is increased at low temperature [27].

III.5. Kinetics of electrolyte degradation and capacity fading

As noticed in Figure 5, the catalytic reaction between LNMO and LP30 is strongly limited at low temperature. This observation led us test the cyclability of LNMO composite electrodes at three different temperatures, 25, 10 & 5°C. The idea is to check if the mitigation of the

electrolyte oxidation, also mitigates the material degradation, i. e. the capacity fading. The results are shown in figure 6.

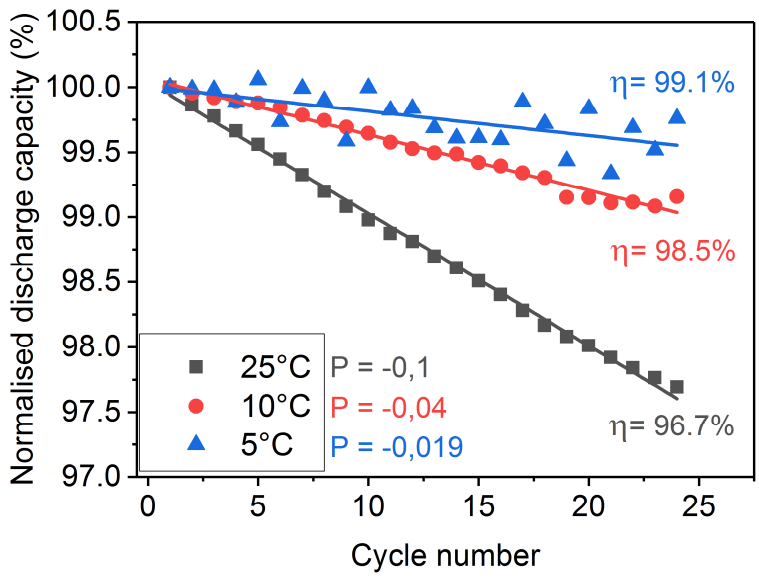

Figure 6: Cyclability (at C/3 D/2) of LNMO composite electrodes at different temperatures : 5, 10 and 25°C. P is the slope of the normalized capacity fading in %/cycle. The associated mean faradic efficiency is specified for each cycling temperature.

When the temperature is lowered, the coulombic efficiency is improved as expected, but the cycling stability is also increased. Thus, there is a strong link between the faradic efficiency linked to the electrolyte oxidation, and what we called a material efficiency, linked to the material degradation. This material efficiency can be expressed as the ratio of the capacity at the cycle n+1 over the capacity at the cycle n, and is also equivalent to 1-|P|, with P the slope of the capacity fade.

$$\eta_{mat} = C_{n+1}/C_n = 1 - |P| \qquad \text{eq. 10}$$

Both faradic and material efficiency are plotted figure 7. It shows a very good correlation between the two, confirming the direct link between the oxidation of the electrolyte and the

degradation of the active material. Therefore, this is not surprising that Wang et al. succeeded to make 800 cycles at 1C rate at 0°C, with only 5% of capacity loss [46].

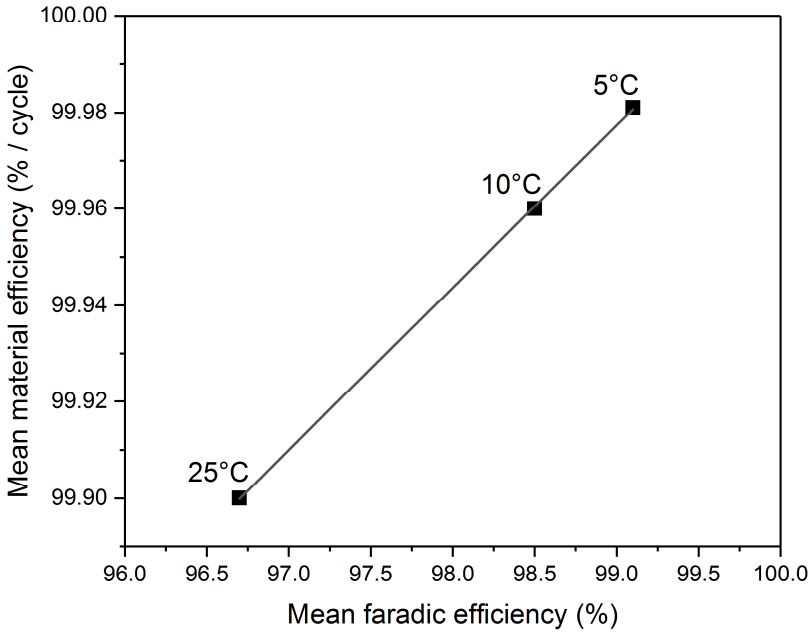

Figure 7 : Mean faradic efficiency vs percentage of capacity loss per cycle for 5, 10 and 25°C (C/3, D/2 rate).

This result strongly support the mechanism proposed by Kostecky et al. [26]: They suggested a mechanism where a cation radical is formed from ethylene carbonate (EC) oxidation by electron transfer from LNMO in oxidized state. The propagation of the radical reaction leads to oligo(ether carbonate) radical that adsorbs at the surface of LNMO. Then a proton-coupled electron transfer leads to the formation of bidentate TM complex. However, our results suggest that only a part of this oxidized solvent molecules can lead to the formation of these complexes, and so to the degradation of the surface of the LNMO. Indeed, we can calculate the number of moles of oxidized electrolyte ($n(E^+)$) molecules using the $i_{0,cor}$ and alpha terms found thanks to eq. 8 and Faraday's law:

$$n(E^+) = (S_{LNMO}/F) \int_0^t i_{0,cor} exp^{(\alpha n F E(t)/RT)}\, dt \qquad \text{eq. 11}$$

It is also possible to access to this value using i_{cor} (assuming eq. 1)

$$n(E^+) = S_{LNMO} \times \int_0^t i_{cor} \times dt/F \approx I_c(1 - \eta_{far}) \times t_c/F \qquad \text{eq. 12}$$

The advantage of eq. 12 is its simplicity because η_{far} can be obtain after a complete cycle charge/discharge, which enables the estimation of the corrosion current.

Assuming that the capacity fading is due to the transition metal Mn/Ni dissolution, we can calculate the number of mole of transition metal n(TM) solvated, from the material efficiency η_{mat}:

$$n(TM) = (I_c\, t_c/F)\,(1 - \eta_{mat}) \qquad \text{eq. 13}$$

Finally, the ratio between the oxidized electrolyte molecules and the TM dissolution can be expressed as:

$$n(TM)/n(E^+) = (1 - \eta_{mat})/(1 - \eta_{far}) \qquad \text{eq. 14}$$

We applied eq. 11 to 14 to a set of experiment at low and moderate rates, and at different temperatures; obtained values are summarized on table 2. First of all, we see that at 25°C both eq. 11 and 12 lead to similar value, which is very satisfactory. We did not measure the of $i_{cor}(E)$ values for 10 and 5°C.

Cycling	$n(E^+)$ using eq. 12	$n(E^+)$ using eq. 11	n(TM)	$n(TM)/n(E^+)$

condition	(mol)	(mol)	(mol)	(%)
C/5, D/5	$4.4x10^{-7}$	$4.3x10^{-7}$	$2x10^{-8}$	4.4
C/2, D	$3.1x10^{-7}$	$2.6x10^{-7}$	$1.1x10^{-8}$	4.2
10°; C/3, D/2	$1.8x10^{-7}$	X	$4.6x10^{-9}$	2.6
5°; C/3, D/2	$9.5\ x10^{-8}$	X	$2\ x10^{-9}$	2.1

Table 2 : Calculated moles number of oxidized electrolyte molecules n(E^+) using eq. 11 or 12, amount of dissolved transition metals n(TM) calculated using eq. 13, and ratio between the two (eq. 14), giving the percentage of oxidized molecules that are correlated with surface TM dissolution.

Then, we saw that lowering the temperature from 25 to 5°C decreases the amount of oxidized molecules from a factor 5, and the active material dissolution from a factor 10. The ratio between the two is around 4%, telling that about 4% of oxidized electrolyte molecules lead to TM dissolution. It may be explained considering that carbonates oxidation leads to several byproducts (alcohol, ketone, ester, ether….), which only a part (i. e. ketanoate [26]) are active actors of the AM dissolution. Also, the byproducts can interact together or with the solvent and salt molecules buffering their chelating properties. This ratio is conserved when the rate is changed, however we observed that it seems to decrease when the temperature is lowered. This can be due to 1/ an imprecise coulometric that leads to some incertitude on the efficiencies, when they reach values close to 100% [47] or 2/due to different thermal activation of electrolyte degradation processes that may disadvantage the formation of ketanoate at lower temperature.

This methodology enables to directly correlate the faradic efficiency and the capacity fading, which permits to rigorously probe the efficiency of an electrolyte additive or AM coating.

Indeed, we applied this calculation on the results of Passerini et al. [15], where they used succinic anhydride as additive to protect the LNMO surface. On the raw material, they obtained a faradic efficiency of 99.3% and a material efficiency of 99.96% for a C/2 rate with a cut-of off 4.95V vs Li^+/Li, leading to a ratio between TM dissolution and oxidized electrolyte of 5.5%, which is quite close to the ≈4% obtained here. It should be noted that their LNMO presents a very low specific surface, with grains of 3 to 5 µm in diameter which, in agreement with our findings i. e. the degradation depends on the active material surface, induces high faradic and material efficiency compared to our synthesis which leads to more divided AM. The addition of succinic anhydride has enabled the increase of both faradic and material efficiencies (99.6 and 99.99%, respectively) by limiting the oxidation of electrolyte, and thus the generation of ketanoate.

Conclusion

High potential cathode as LNMO suffers from a low coulombic efficiency and continuous capacity fading. The average working potential of these electrodes (4,7-4,8 V vs Li+/Li) is superior to the stability window of conventional carbonate based electrolytes. This leads to the oxidation of the electrolyte when using a commercial LP30 electrolyte (EC/DMC 1M $LiPF_6$), which appears to be the mean reason for the low coulombic efficiency of LNMO. This oxidation is temperature and potential activated and follows a Tafel dependence. In addition, it has been proved that this oxidation mechanism is catalyzed by the active material surface, and that the oxidation of the electrolyte on the carbon has only a minor contribution to the total corrosion current. Our electrochemical approach confirms that a simple model based on the faradic efficiency enables the fast determination of a corrosion current (density) that is close to the one measured by potentiostatic methods or self-discharge experiments.

In parallel, it has been shown that a fluorinated environment does not significantly impact the capacity loss, leading us to conclude that HF generation (due to the degradation of $LiPF_6$ or PVDF) is not the main raison for AM degradation, as commonly believed. In contrast, a strong link between the kinetics of the electrolyte oxidation and the kinetics of AM degradation has been demonstrated, which support the idea that the mitigating of the electrolyte oxidation would lower the capacity fading leading to improved LNMO cycle life. We develop a methodology which allows to quantify the ratio between the AM degradation and the electrolyte degradation. It could be used to discriminate the different approaches to improve the interfacial stability such as the use of additives to buffer the LNMO surface or ex-situ surface coating. Finally, in terms of materials chemistry, our findings demonstrate that the use of large LNMO grains which minimizes the electro-catalytic active surface would be a first step [48], [13], [15]. A coating based on carbon would be a very interesting approach thanks to its very limited catalytic activity for electrolyte oxidation [49], [50], [41], [42].

Acknowledgment:

We would like to thanks Institut Carnot Energie du Futur for its funding of work through the project Prolion.

References

[1] H. L. C. E. G. G. L. S. G. S. Z. K. .. &. G. N. Zhang, “From Solid-Solution Electrodes and the Rocking-Chair Concept to Today's Batteries.,” *Angewandte Chemie International Edition,* pp. 534-538, 2020.

[2] A. &. E. Y. Kraytsberg, “Higher, Stronger, Better… A Review of 5 Volt Cathode Materials for Advanced Lithium-Ion Batteries.,” *Advanced Energy Materials,* pp. 2(8), 922-939., 2012.

[3] B. Q. D. W. Z. &. M. Y. S. Xu, “Recent progress in cathode materials research for advanced lithium ion batteries.,” *Materials Science and Engineering: R: Reports,* pp. 51-65, 2012.

[4] Q. B. A. Z. M. G. Y. &. D. J. R. Zhong, “Synthesis and Electrochemistry of LiNixMn2-xO4,” *Journal of The Electrochemical Society,* p. 205, 1997.

[5] Y. Y. K. N. F. K. T. Y. M. &. N. I. Terada, “In situ XAFS analysis of Li(Mn,M)2O4 (M= Cr, Co, Ni) 5V cathode materials for lithium-ion secondary batteries.,” *Journal of Solid State Chemistry,* pp. 156(2), 286-291, 2000.

[6] G. B. W. Y. Y. Z. Z. C. &. C. C. H. Zhong, “Effects of Al substitution for Ni and Mn on the electrochemical properties of LiNi0. 5Mn1. 5O4,” *Electrochimica Acta,* pp. 56(18), 6554-6561., 2011.

[7] M. B. D. D. T. C. D. V. K. G. T. B. R. J. &. P. S. Kuenzel, “Complementary Strategies Toward the Aqueous Processing of High-Voltage LiNi0.5Mn1.5O4 Lithium-Ion Cathodes.,” *ChemSusChem,* pp. 562-573, 2018.

[8] L. L. F. G. P. Y. &. C. A. Barbosa, “Simple and eco-friendly fabrication of electrode materials and their performance in high-voltage lithium-ion batteries.,” *ChemSusChem,* 2019.

[9] M. &. A. G. G. Kunduraci, “Synthesis and Characterization of Nanostructured 4.7 V LixMn1.5Ni0.5O4 Spinels for High-Power Lithium-Ion Batteries,” *Journal of the Electrochemical*

Society, pp. 153(7), A1345-A1352., 2006.

[10] J. H. X. Z. X. C. F. &. C. J. Yang, “Spinel LiNi0.5Mn1.5O4 cathode for rechargeable lithiu mion batteries: Nano vs micro, ordered phase (P4332) vs disordered phase (Fd3m),” *Nano Research,* pp. 6(9), 679-687., 2013.

[11] Y. S. Y. &. H. X. Chen, “Origin of the Ni/Mn ordering in high-voltage spinel LiNi0.5Mn1.5O4: the role of oxygen vacancies and cation doping,” *Computational Materials Science,* pp. 109-116, 2016.

[12] N. Z. K. G. F. M. A. &. J. C. M. Amdouni, “Structure and insertion properties of disordered and ordered LiNi0.5Mn1.5O4 spinels prepared by wet chemistry.,” *Ionics,* pp. 117-126, 2006.

[13] J. C. X. Y. F. X. G. L. S. S. Y. L. J. T. H. L. &. S. S. G. Fang, “Fabrication of densely packed LiNi0.5Mn1.5O4 cathode material with excellent long-term cycleability for high-voltage lithium ion batteries.,” *Journal of Power Sources,* pp. 304, 15-23., 2016.

[14] S. S. D. K. A. S. F. J. S. H. M. .. &. P. H. Yang, “Electrochemical and electronic charge transport properties of Ni-doped LiMn2O4 spinel obtained from polyol-mediated synthesis,” *Materials,* pp. 11(5), 806., 2018.

[15] V. K. J. N. M. B. D. P. L. F. F. .. &. P. S. Tarnopolskiy, “Beneficial influence of succinic anhydride as electrolyte additive on the self-discharge of 5 V LiNi0.4Mn1.6O4 cathodes,” *Journal of Power Sources,* pp. 236, 39-46., 2013.

[16] N. P. L. Z. L. P. O. K. L. M. J. P. B. R. &. K. J. H. Pieczonka, “Understanding transition-metal dissolution behavior in LiNi0. 5Mn1. 5O4 high-voltage spinel for lithium ion batteries.,” *The Journal of Physical Chemistry C,* pp. 117(31), 15947-15957., 2013.

[17] Z. Z. R. D. P. H. H. W. T. Z. L. &. C. H. Chen, “Polyhedral LiNi0.5Mn1.5O4 with excellent electrochemical properties for lithium-ion batteries,” *Journal of Materials Chemistry A,* pp. 2(32), 12835-12848, 2014.

[18] S. X. M. K. B. &. L. B. L. Dalavi, “Effect of added LiBOB on high voltage (LiNi0.5Mn1.5O4) spinel cathodes,” *Electrochemical and Solid State Letters,,* p. A28, 2011.

[19] Y. V. G. M. B. K. L. C. J. H. D. K. P. M. P. .. &. S. X. G. Li, “Lithium malonatoborate additives enabled stable cycling of 5 V lithium metal and lithium ion batteries.,” *Nano Energy,* pp. 9-19, 2017.

[20] J. W. K. D. H. O. D. Y. L. H. K. J. H. L. J. H. &. J. Y. S. Kim, “Surface chemistry of LiNi0.5Mn1.5O4 particles coated by Al2O3 using atomic layer deposition for lithium-ion batteries.,” *Journal of power sources,* pp. 274, 1254-1262., 2015.

[21] T. F. M. J. &. Z. Y. R. Yi, “Key strategies for enhancing the cycling stability and rate capacity of LiNi0.5Mn1.5O4 as high-voltage cathode materials for high power lithium-ion batteries.,” *Journal of power sources,* pp. 85-105, 2016.

[22] J. J. P. W. K. &. W. S. H. Shiu, “Preparation and characterization of spinel LiNi0.5-xMgxMn1.5O4 cathode materials via spray pyrolysis method.,” *Journal of power sources,* pp. 35-42, 2013.

[23] J. &. M. A. Liu, “Understanding the improved electrochemical performances of Fe-substituted 5 V spinel cathode LiMn1.5Ni0.5O4,” *The Journal of Physical Chemistry C,* pp. 15073-15079, 2009.

[24] K. Xu, “Nonaqueous liquid electrolytes for lithium-based rechargeable batteries,” *Chemical reviews,* pp. 4303-4418, 2004.

[25] N. L. K. &. S. D. J. Kumar, “Crystal surface and state of charge dependencies of electrolyte decomposition on LiMn2O4 cathode,” *Journal of The Electrochemical Society,* pp. E3059-E3065,

2014.

[26] A. G. S. Y. Y. S. R.-R. J. K. C. C. J. .. &. K. R. Jarry, “The Formation Mechanism of Fluorescent Metal Complexes at the LixNi0.5Mn1.5O4-δ/Carbonate Ester Electrolyte Interface,” *Journal of the American Chemical Society,* pp. 137(10), 3533-3539., 2015.

[27] M. B.-R. L. B. P. T. C. N. P. V. C. &. B. E. J. He, “Effects of Solvent, Lithium Salt, and Temperature on Stability of Carbonate-Based Electrolytes for 5.0 V LiNi0.5Mn1.5O4 Electrodes,” *Journal of The Electrochemical Society,* pp. 163(2), A83-A89., 2016.

[28] X. L. X. W. Z. G. H. &. Y. P. Wu, “Capacity fading reason of LiNi0.5Mn1.5O4 with commercial electrolyte.,” *Ionics,* pp. 19(2), 379-383, 2013.

[29] T. P. S. M. J. R. J. H. C. W. K. Y. S. .. &. O. S. M. Yoon, “Failure mechanisms of LiNi0.5Mn1.5O4 electrode at elevated temperature,” *Journal of power sources,* pp. 215, 312-316., 2012.

[30] W. K. L. C. Z. L. C. E. P. V. K. L. H. F. L. S. C. &. C. J. M. Pang, “Crystallographic origin of cycle decay of the high-voltage LiNi0.5Mn1.5O4 spinel lithium-ion battery electrode,” *Physical Chemistry Chemical Physics,* pp. 18(26), 17183-17189., 2016.

[31] J. H. P. C. G. &. C. L. Ma, “Surface and interface issues in spinel LiNi0.5Mn1.5O4: insights into a potential cathode material for high energy density lithium ion batteries.,” *Chemistry of Materials,* pp. 3578-3606, 2016.

[32] J. L. D. C.-C. M. G. H. &. C.-M. B. Demeaux, “New insights into a high potential spinel and alkylcarbonate-based electrolytes.,” *Electrochimica Acta,* pp. 89, 163-172., 2013.

[33] M. M. K. D. T. I. I. U. M. Mohamedi, “Electrochemical investigation of LiNi0.5Mn1.5O4 thin film,” *electrochimica acta,* pp. 79-84, 2002.

[34] M. G. K. I. Z. J. O. A. S. S. Y. C. .. &. R. B. Gellert, “LiNi0.5Mn1.5O4 thin-film cathodes on gold-coated stainless steel substrates: formation of interlayers and electrochemical properties.,” *Electrochimica Acta,* pp. 146-152, 2014.

[35] J.-H. Kim, S.-T. Myung, C. S. Yoon, S. G. Kang and Y.-K. Sun, “Comparative study of LiNi0.5Mn1.5O4–δ and LiNi0.5Mn1.5O4 cathodes having two crystallographic structures: Fd3m and P4332,” *Chem. Mater.,* pp. 16, 906–914, 2004.

[36] K. M. M. A. N. I. T. &. U. I. Dokko, “In situ Raman spectroscopic studies of LiNixMn2-xO4 thin film cathode materials for lithium ion secondary batteries,” *Journal of Materials Chemistry,* pp. 3688-3693, 2002.

[37] L. V. C. B. P. T. C. N. P. &. B. Y. M. Boulet-Roblin, “Versatile approach combining theoretical and experimental aspects of Raman spectroscopy to investigate battery materials: the case of the LiNi0. 5Mn1. 5O4 spinel,” *The Journal of Physical Chemistry C,* pp. 16377-16382, 2016.

[38] S. E. P. H. &. T. E. Brunauer, “Adsorption of gases in multimolecular layers,” *Journal of the American chemical society,* pp. 309-313, 1938.

[39] Y. C. L. &. W. R. E. Dai, “Capacity fade model for spinel LiMn2O4 electrode,” *Journal of The Electrochemical Society,* pp. A182-A190, 2013.

[40] L. R. B. &. L. B. L. Yang, “Electrolyte reactions with the surface of high voltage LiNi0.5Mn1.5O4 cathodes for lithium-ion batteries,” *Electrochemical and Solid-State Letters,* pp. A95-A97, 2010.

[41] X. G. M. R. J. &. Z. C. Fang, “Graphene-oxide-coated LiNi0.5Mn1.5O4 as high voltage cathode for lithium ion batteries with high energy density and long cycle life,” *Journal of Materials Chemistry A,* pp. 1(12), 4083-4088, 2013.

[42] H. S. Z. L. J. Y. S. R. R. C. J. .. &. Z. B. Wang, “Direct carbon coating at high temperature on LiNi0.5Mn1.5O4 cathode: Unexpected influence on crystal structure and electrochemical performances.,” *Journal of Power Sources,* pp. 288, 206-213, 2015.

[43] C. A. C. H. J. L. J. H. Y. S. Y. K. J. W. S. J. H. &. K. B. Kim, “Influence of surface modification on electrochemical performance of high voltage spinel ordered-LiNi0.5Mn1.5O4 exposed to 5.3 V for 100h before and after surface modification with ALD method,” *Electrochimica acta,* pp. 134-142, 2015.

[44] Q. Y. Y. S. S. Z. X. W. N. &. B. Y. Wu, “Novel AlF3 surface modified spinel LiMn1. 5Ni0. 5O4 for lithium-ion batteries: performance characterization and mechanism exploration,” *Electrochimica Acta,* pp. 73-80, 2015.

[45] M. C. M. G. H. E. &. A. D. Moshkovich, “The study of the anodic stability of alkyl carbonate solutions by in situ FTIR spectroscopy,” *Journal of Electroanalytical Chemistry,* pp. 84-96, 2001.

[46] J. N. P. X. G. J. J. W. Y. F. R. .. &. Z. X. Wang, “High-Voltage LiNi0.45Cr0.1Mn1.45O4 Cathode with Superlong Cycle Performance for Wide Temperature Lithium-Ion Batteries,” *Advanced Functional Materials,* pp. 28(4), 1704808, 2017.

[47] A. W. C. J. M. E. &. D. J. R. Rowe, “High Precision Coulometry Studies of Single-Phase Layered Compositions in the Li-Mn-Ni-O System,” *Journal of The Electrochemical Society,* p. A1189, 2014.

[48] Y. M. B. L. R. S. G. A. D. K. D. .. &. S. R. Talyosef, “Comparing the behavior of nano-and microsized particles of LiMn1. 5Ni0. 5O4 spinel as cathode materials for Li-ion batteries.,” *Journal of the Electrochemical Society,* pp. 154(7), A682-A691., 2007.

[49] N. Y. T. L. Y. &. S. K. Zhang, “A facile method to prepare hybrid LiNi0.5Mn1.5O4/C with enhanced rate performance,” *Journal of Alloys and Compounds,* pp. 509(9), 3783-3786., 2011.

[50] T. Z. N. L. Y. &. S. K. Yang, " Enhanced rate performance of carbon-coated LiNi0.5Mn1.5O4 cathode material for lithium ion batteries," *Electrochimica Acta,* pp. 56(11), 4058-4064., 2011.

[51] Y. S. X. H. Yuyang Chen, "Origin of the Ni/Mn ordering in high-voltage spinel LiNi0.5Mn1.5O4: The role of oxygen vacancies and cation doping," *Computational Materials Science,* pp. 109-116, 2016.

[52] A. L. D. L. Y. K. K. &. S. Y. Ito, "Influence of Co substitution for Ni and Mn on the structural and electrochemical characteristics of LiNi0.5Mn1.5O4," *Journal of Power Sources,* pp. 185(2), 1429-1433., 2008.

[53] M. D. K. &. K. K. Matsui, "Surface Layer Formation and Stripping Process on LiMn2O4 and LiNi1⁄2Mn3⁄2O4 Thin Film Electrodes.," *Journal of The Electrochemical Society,* pp. 157(2), A121-A129., 2010.

[54] H. M. Y. S. L. L. &. C. G. Xia, "Electrochemical properties of nonstoichiometric LiNi0.5Mn1.5O4-δ thin-film electrodes prepared by pulsed laser deposition," *Journal of the Electrochemical Society,* pp. 154(8), A737-A743., 2007.

[55] Y. W. Z. Z. L. Y. F. L. B. Z. Y. &. K. K. Xue, "Investigation on preparation and performance of spinel LiNi0.5Mn1.5O4 with different microstructures for lithium-ion batteries," *Scientific reports,* pp. 5, 13299., 2015.

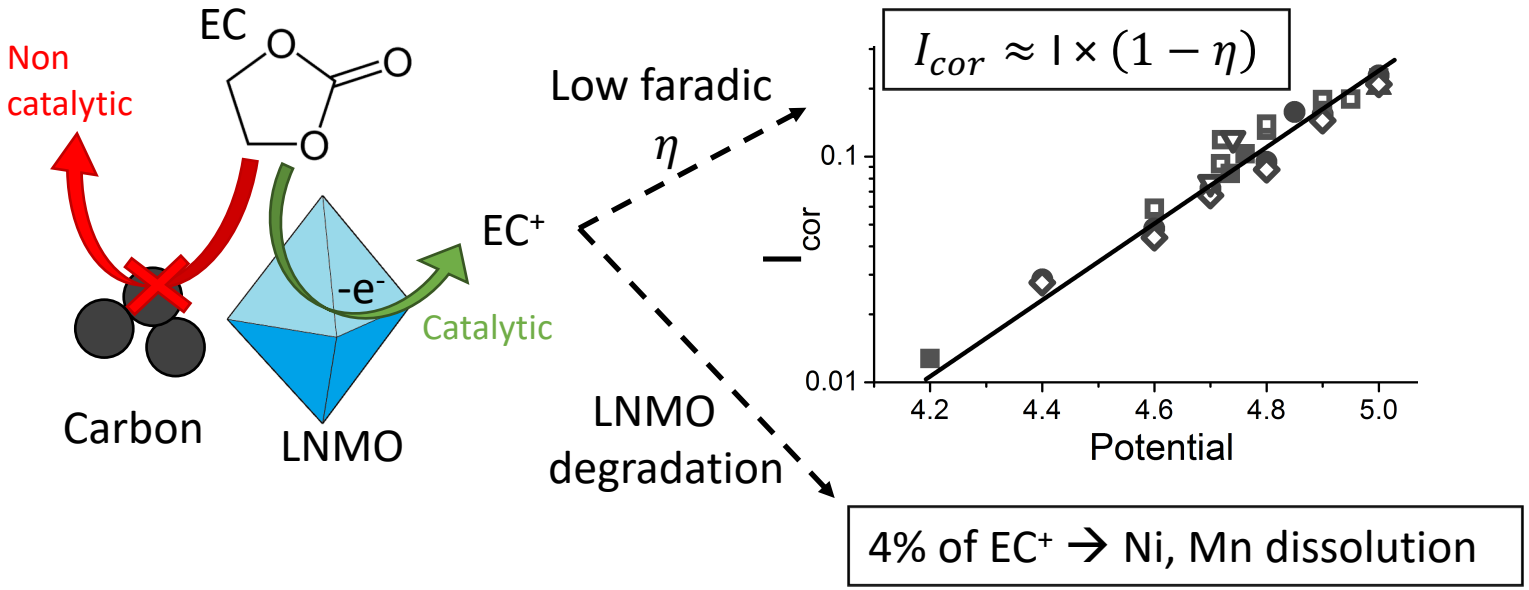
EC
Non
catalytic
-e⁻
Catalytic
Carbon
LNMO
Low faradic
η
EC⁺
LNMO
degradation
$I_{cor} \approx I \times (1 - \eta)$
0.1
0.01
I cor
4.2
4.4
4.6
4.8
5.0
Potential
4% of EC⁺ → Ni, Mn dissolution